

Mapping the mechanics and macromolecular organization of hyaluronan-rich cell coats†

Heike Boehm,^{*a} Tabea A. Munding,^a Christian H. J. Boehm,^a Valentin Hagel,^a Uwe Rauch,^b Joachim P. Spatz^a and Jennifer E. Curtis^{ac}

Received 20th March 2009, Accepted 14th July 2009

First published as an Advance Article on the web 7th September 2009

DOI: 10.1039/b905574f

The hyaluronan (HA)-rich pericellular coat (PCC) enveloping most mammalian cells plays a vital role in biological processes such as cell adhesion, proliferation, motility and embryogenesis. In particular its presence on chondrocytes, which live in the load-bearing cartilage, has a wide range of implications in diseases such as osteoarthritis, highlighting its mechanical role in living organisms. Despite its significance, the macromolecular organization of the cell coat remains speculative. In order to obtain a more detailed spatial picture of highly hydrated PCCs, we present two independent but complementary non-invasive techniques for the position-resolved analysis of the cell coat's mechanical and structural properties. Position-dependent microrheology provides a micromechanical map of the PCC that reveals a gradient of increasing elastic stiffness towards the plasma membrane on model rat chondrocyte cells (RCJ-P). This gradient can be correlated with the relative distribution of HA, which is inferred using an eGFP-labelled neurocan-binding domain, a small fluorescent molecule that binds to HA. The spatial variation of the HA concentration profile is consistent with the position-dependent elasticity. Combining these approaches sheds light on the molecular architecture of the PCC.

Introduction

Most mammalian cells are enveloped by a coat of polysaccharides and proteins.¹ This coat influences vital biological processes such as cell adhesion,² proliferation,^{3,4} motility^{5,6} and embryogenesis.⁷ The constitution and thickness of this layer, referred to as the pericellular coat (PCC), pericellular matrix or glycocalyx, can vary considerably. Here we focus on cell coats whose vital structural backbone is hyaluronan (HA), a highly hydrated polysaccharide that anchors the coat to the cell membrane.⁸ The molecular interaction of HA with different HA-binding proteins^{9,10} determines the architecture of the PCC.^{11,7} The resultant mesoscopic arrangement of the different PCC components influences the cell's perception of the extracellular environment and its ability to withstand compression.¹² The stress transduction through the PCC is especially important for chondrocytes, cells located in the load-bearing cartilage. The molecular structure of some PCC components, especially the HA-binding protein aggrecan, changes with age^{13,14} or osteoarthritis.¹⁵ These changes alter the viscoelasticity of the PCC and may also affect its molecular architecture. Currently, few if any

methods exist that characterize these mesoscopic changes in the PCC induced by age, sickness or therapeutic treatments.

Analysis of the PCC has proven to be very difficult due to its high water content which renders it invisible to optical microscopy techniques. One indirect approach to understanding PCC structure is to measure its mechanical properties. So far all mechanical measurements of the PCC necessarily include contributions from the cell body which do not originate from the cellular coat. Therefore, complex mathematical analysis is required to decouple this influence from the simultaneously measured cell body. Strain apparatus^{16,17} and micropipette aspiration^{18,19} experiments obtained values for the average Young's moduli of individual PCCs that indicate a mechanical difference between arthritic and normal human chondrocytes. An alternative AFM-based approach evaluates mean PCC elasticity at different locations on the cell.^{20–22} However, it too is influenced by the underlying cell body, requiring theoretical assumptions to interpret the data. Thus, we generally lack techniques that provide details about the spatial variations in the hyaluronan distribution or about the varying mechanics throughout the PCC.

Here we employ a combination of microrheology and quantitative confocal fluorescent microscopy on the PCC of living rat chondrocyte cells (RCJ-P), which serve as a well-established model system for HA-rich coats.^{23,2} We establish the first micromechanical map of the PCC, using passive particle tracking microrheology,^{24,25} which reveals an increase in both the viscosity and the elasticity of the PCC towards the cell surface. Further, we characterize the distribution of HA and observe a linear increase in fluorescence intensity towards the cell membrane. Comparing the results of these approaches using polymer theory sheds light on the macromolecular architecture of the PCC. Our data

^aMax-Planck-Institute for Metals Research, Department New Materials & Biosystems and University of Heidelberg, Department of Biophysical Chemistry, Heisenbergstr. 3, 70569 Stuttgart, Germany. E-mail: hboehm@mf.mpg.de; Fax: +49 711 689 3612; Tel: +49 711 689 3622

^bVessel Wall Biology, Department of Experimental Medical Science, Biomedical Center, Lund University, 221 84 Lund, Sweden

^cSchool of Physics, Georgia Institute of Technology, 837 State Street, Atlanta, GA, 30332-0430, USA

† Electronic supplementary information (ESI) available: Uniform GFPn fluorescent HA profiles versus cell height and scanning electron micrograph (SEM) image of cell microvilli. See DOI: 10.1039/b905574f

indicate that the structure of PCC is far more complex than expected from a pure end-grafted polymer brush.

Results

Micromechanical mapping of the PCC

Passive particle tracking microrheology is a non-invasive approach to measuring the local mechanical properties of microscopic volumes of material including polymer solutions, the cytoplasm, or even, as we demonstrate here, the pericellular coat. Based on the simple video detection of the thermal motions of added tracer particles, a statistical analysis of the Brownian motion (see Materials and methods) can be used to derive the viscoelastic properties of the surrounding media. Here we conduct a position-dependent analysis of the tracers' thermal fluctuations to extract a micromechanical map of the PCC without perturbing the cell or its coat.

As a first step to establish a working microrheology protocol within the cell coat, we demonstrated that particles freely diffuse into and out of the PCC over longer periods of time, confirming that they are not irreversibly bound to PCC components. This was further validated by control microrheology (MR) experiments in pure HA solutions, which yielded results consistent with literature values.²⁶

We then systematically mapped the micromechanical properties of the PCC along the direction perpendicular to the cell surface by spatially resolving the Brownian motion of 0.45 μm tracer particles. The position of each tracer particle was determined with respect to the plasma membrane and the edge of the PCC in terms of the particle's relative position, $p = d/t$. Here, d is the absolute distance to the cell membrane, as measured from the fluorescent intensity peak of the WGA555-stained membrane and t is the coat thickness, measured by particle exclusion assays (PEAs). This assay indirectly visualizes the extent of the highly hydrated coat *via* the exclusion of erythrocytes (red blood cells) from the PCC volume. The thickness of the PCC had typical values ranging from 3 to 8 μm .

Typically particles move about their mean position to an extent characterized by the average radius of gyration, which is 0.45 μm (st. dev. 0.24 μm). Examination of their trajectories revealed continuous diffusion without trapping events.²⁷ Their diffusion in a viscoelastic solution can be characterized by the lag time (τ)-dependent mean-square displacement (MSD), which can be related to the diffusion constant (D) in n dimensions by:²⁴

$$\text{MSD}(\tau) = 2n \times D \times \tau^\alpha \quad (1)$$

The diffusive exponent, α , is related to the ratio of elastic and viscous contributions of the solution such that $\alpha = 1$ in viscous and $\alpha = 0$ in purely elastic solutions, whereas $\alpha = 0.5$ at the gel point²⁸ and $\alpha > 1$ for superdiffusion arising in active processes. Furthermore, under appropriate conditions (see Discussion), the MSD can be related to the elastic storage modulus, G' , and the viscous loss modulus, G'' , for comparison with reference to ideal bulk solution values (see eqn (3) and (4)).

The average diffusive exponent $\alpha = 0.964$ at a distance of $2 < p < 4$ indicates that tracer particles diffuse freely and the sample behaves like a Newtonian fluid at distances at least two times the PCC thickness. Furthermore, we obtained a viscosity of

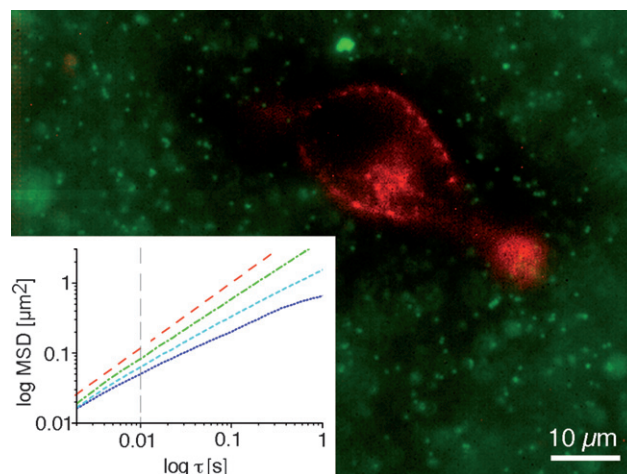


Fig. 1 The Brownian motion of fluorescent tracer particles (green) in close proximity to a cell (membrane stained in red with WGA555) was observed 4 μm above the glass slide, where we analyzed the position of each particle within the PCC and the corresponding viscoelasticity around it. The viscoelasticity is given by the mean-squared displacement (MSD) characterizing the diffusion of the particles in pure media (orange, dashed), at the edge of the PCC at a relative position of $p = 1.0\text{--}0.7$ (green, dashed dots), at $p = 0.7\text{--}0.4$ (cyan, small dashed) and close to the cell at $p = 0.4\text{--}0.1$ (blue, straight). The stiffness of the PCC increases as the value of the MSD decreases. Additionally the elasticity increases as the double-logarithmic slope decreases.

7.25×10^{-4} Pa s at these distances, which agrees well with the viscosity of water at 37 $^{\circ}\text{C}$.

Inside the cell coat, variation of the viscoelasticity is indicated by slower motion of tracer particles and their corresponding smaller MSDs as they approach the cell surface (Fig. 1). To characterize this decrease, we plotted the MSD value at a specific lag time ($\tau = 0.01$ s) against the entire range of relative positions and observed a linear decrease (Fig. 1, inset and Fig. 2a). Similarly, the diffusive exponent within the PCC also decreases linearly towards the cell membrane: $\alpha = 0.492 + 0.443p$ for $0 < p < 1$, illustrating the increasing elasticity of the PCC up to the gel point of $\alpha = 0.5$ (Fig. 2b). The standard deviation of α arising from different cells was 0.097, indicating that cell to cell variances are of minor importance.

Identical experiments were performed and analyzed for hyaluronidase-treated cells. No measurable change in MSD or diffusive exponent was detected, indicating that our results from non-hyaluronidase-treated cells are due to the hyaluronan-rich PCC.

GFPn-labeling of hyaluronan within the PCC

We characterized the HA distribution in the pericellular coat using an eGFP-labelled neurocan-binding domain (GFPn), an eGFP fusion protein developed by Zhang and co-workers that specifically labels HA,²⁹ similar to the two-component protein probe developed by Tammi and co-workers.⁸ In preparation for quantitative measurements of the HA concentration profile in the cell coat, possible structural changes in the PCC induced by GFPn were assessed using particle exclusion assays (PEAs). These studies verified that PCC thickness is not altered by the addition of

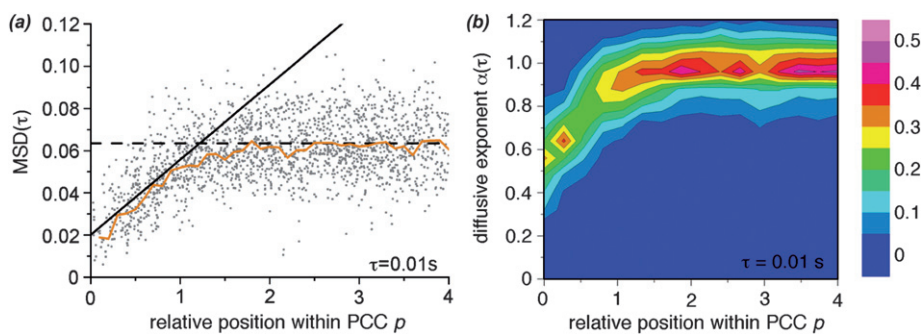


Fig. 2 The mechanical properties of the PCC change gradually towards the cell membrane. (a) The decreasing MSD value depicts an increasing stiffness throughout the PCC. Each grey spot corresponds to one tracer, where there are about 350 tracers within the PCC on 11 different cells on 11 different samples. The orange line corresponds to the weighted average MSD. The black dashed line depicts a linear fit of the data from $p = 2$ to $p = 4$ and the black solid line depicts the linear fit between 0 and 1: $\text{MSD} = 0.020 + 0.036p$. (b) The diffusive exponent α characterizes the ratio of viscous and elastic contributions to the viscoelasticity of the PCC. As pure media is purely viscous, the elastic component is consistently increased towards the cell membrane. The distribution at the different positions is broadened by the statistical thermal noise. The width of the distribution within the PCC is reduced compared to that in media due to the damped thermal motion of particles within the PCC.

GFPn. Further to prove that GFPn binds exclusively to HA, the cells were treated with hyaluronidase, an enzyme that only digests HA which completely removes the PCC without adversely affecting the cells. No GFPn signal was observed when GFPn was added after such a treatment. The specific binding of GFPn to HA can also be controlled by specifically blocking GFPn with short HA (of a unit length of 8 disaccharides). GFPn blocked with short HA does not lead to a fluorescent staining of the PCC.

Analysis of fluorescent images acquired with spinning disk confocal microscopy revealed the presence of PCC on all membrane areas not in contact with the glass surface, including the apical region of living RCJ-P cells. Position-dependent intensity profiles of GFPn-labelled HA were measured along the coordinate perpendicular to the plasma membrane (Fig. 3a) and summed over $1 \mu\text{m}$ generating highly reproducible intensity profiles such as the typical curve shown in Fig. 3b. We find that the HA intensity profile peaks in an area co-localized with the membrane (orange, Fig. 3a) and decreases in the direction towards the rim of the PCC. The initial sharp increase in intensity (orange, Fig. 3b) over $1.8 \pm 0.5 \mu\text{m}$ overlaps with the membrane staining, with a maximum corresponding to the membrane edge. This unintuitive variation of GFPn at the cell surface is a side effect of the small microvilli which we have visualized in SEM images taken after critical point drying (ESI†). This explains the roughness of the membrane edge which co-localizes with GFPn-labelled HA and which can be related to the thickness of the microvilli layer ($1.8 \pm 0.5 \mu\text{m}$). Outside of this critical area, the GFPn intensity decreases with the same functional form, independent of membrane curvature and at different cell heights from the substrate (see ESI†).

In order to examine the dependence of the HA concentration profiles to the total coat thickness, t , we compared the spatial variations of GFPn intensity profiles at $4 \mu\text{m}$ above the glass surface from multiple cells. We performed a linear fit to several intensity profiles, $I(d) = md + I(0)$, where m is the slope, I is the intensity and d is the distance to the membrane in microns. We also tried to fit an exponential decay to the data, which failed due to the high noise ratio at low fluorescence intensity away from the cell membrane. These fits led to the interesting observation that the gradient, m , correlates with the inverse of the PCC thickness:

$m = s \times t^{-1}$ (Fig. 3c). This implies that the distribution of HA through the PCC scales with the thickness of the cell coat. Thus, we find that normalizing the position, d , in the intensity profiles

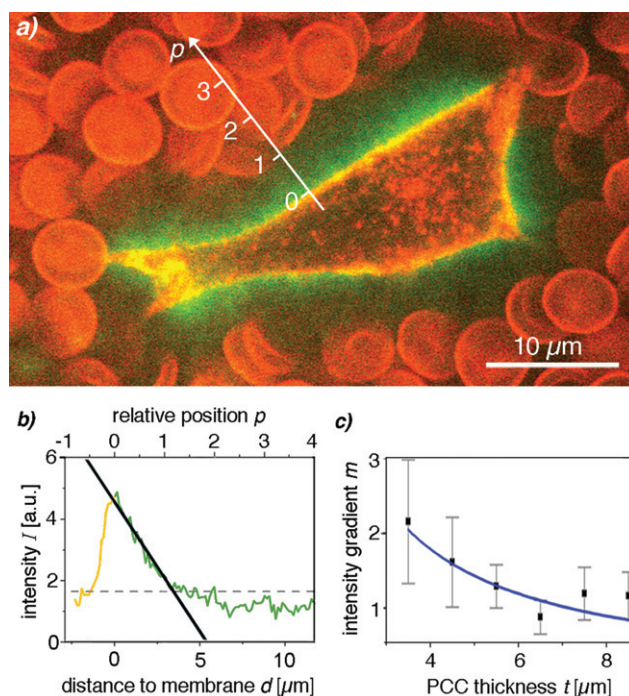


Fig. 3 The fluorescent intensity of GFPn-stained hyaluronan (green) decreases towards the edge of the pericellular coat (PCC), which is delineated by the DiI stained erythrocytes (red) in the particle exclusion assay (PEA). The plasma membrane was labelled with WGA555 (red). (a) Image taken on a spinning disk confocal microscope of a living cell. The membrane is defined as zero and the edge of the PCC determined by the PEA is set to $p = 1$. (b) GFPn intensity profile along the white line in (a) at $4 \mu\text{m}$ above the glass surface with linear fit $I_{\text{fit}} = md + I(0)$ (black) of green data points above the noise level (grey dashed). (c) Average over 75 cells with standard deviations depicted as error bars: the linear decrease in fluorescent intensity (characterized by its slope m) is inversely related to the PEA-determined thickness t of the PCC. Blue fit: $m = s \times t^{-1}$ where s corresponds to the average maximum GFPn intensity.

by the PCC thickness, t , by introducing the relative coordinate $p = dt$, leads to similar intensity profiles.

In the following section, we examine whether this rescaling also applies to our spatially resolved mechanical measurements of the PCC and then use it to relate the concentration profile to the mechanics using polymer theory.

Discussion

We characterized the HA distribution of the PCC with neurocan-GFP in spinning disk confocal microscopy and employed microrheology in a position-sensitive manner to obtain a micromechanical map of the PCC. Both techniques can be applied unobtrusively within the PCC of living cells. Thus, these tools are extremely well suited for the study of the macromolecular architecture of extended polymer layers and for comparing differences in PCCs without uncertainty arising from simultaneous measurement of the adjacent cell body.

Microrheology within the PCC

Passive particle tracking microrheology is an ideal technique for studying the properties of soft materials. For its successful application, several criteria must be fulfilled. First, the thermal motion of the particles has to be visualized. This depends on the softness of the material—which should not constrict the particles too much—and on the equipment used. The vigorous motion of particles in solutions such as water or the PCC requires a high speed camera to obtain enough statistics before they move out of the field of focus. Secondly, the tracers have to be homogeneously distributed within the sample without altering it. Therefore, we allowed particles to diffuse into the PCC, thus neither the cell nor the PCC is perturbed. Since particles diffuse all the way to the cell on non-repetitive tracks, no large scale structures seem to be present on the time scale of observation. This also indicates that the hyaluronan is not strongly cross-linked to form a net with a mesh size lower than the particle diameter of 450 nm. In order to relate the MSD from single particle tracking microrheology to bulk rheological properties, *i.e.* the loss and storage moduli, the tracer particle diameter must be sufficiently larger than the correlation length of the polymer solution.²⁴ If the polymers are not crosslinked, this length depends on the concentration and the length of the polymers, and it is also referred to as mesh size. For an unknown system such as the cell coat, the mesh size is not predictable *a priori*. Thus measurements using several particle sizes are ideal in order to confirm that this criterion is satisfied. Measurements of the cell coat are further complicated by the fact that the mesh size presumably changes with distance to the cell surface. For this preliminary study, we have used 450 nm particles. We therefore neglect to provide quantitative estimates of G' and G'' , which even with verification of the relative size, the limited statistics and typical conversion errors ($\sim 15\%$)³⁰ would allow only an estimate of the values. Thus, instead of calculating the bulk viscoelasticity, we focus on a comparative analysis of the averaged MSD value and the diffusive exponent over all particles with the same relative position at a given lag time. In addition to mapping of different spatial regions, it could also be employed to compare the PCCs of different cell populations.

Microrheology experiments are intrinsically sensitive to any kind of distortion affecting the motion of particles. The sample was therefore equilibrated for 15 min before the start of the experiment and particles far away from the cell always served as controls to check for flow within the sample. Motions of the cell attached to the measured PCC had a negligible influence, as demonstrated by constant viscoelastic profiles on living, hyaluronidase-treated cells, which showed no changes in the diffusive exponent or in the MSD value. Since no motor proteins have been reported inside the PCC, active processes such as those present inside the cells do not have to be considered here.

Comparison of concentration and viscoelasticity profiles

Our first glimpse inside the hydrous pericellular coat with the two independent techniques revealed unexpected spatial profiles of both the hyaluronan distribution and the micromechanical properties. The profiles obtained with these two techniques can be qualitatively compared using polymer theory to relate the local polymer concentration to the MSD. Several publications have validated the relation between the modulus G and concentration for HA and HA–aggrecan solutions given by the modified Rouse model: $G = cRT/M$.^{31,32} We also know that the modulus is inversely related to the mean-squared displacement, where $G \approx 1/\text{MSD}$.³⁰ Thus, we expect that the HA concentration and the MSD spatial profiles can be related by an inverse relationship: $c \approx 1/\text{MSD}$ where both depend on the relative position, p .

For comparison, the data are plotted in Fig. 4, with the caveat that we have not experimentally verified that the particle size is larger than the local mesh size, justifying the use of G . Remarkably, the micromechanical map corresponds well to the measured hyaluronan distribution, except for the MSD values very close to the cell membrane. The disagreement near the cell surface may arise from the breakdown of the polymer theory relating the concentration and the MSD near surfaces with grafted polymers.

In this paper, we consistently identify the edge of the PCC using results from our particle exclusion assays. However, the GFPn intensity appears to indicate a smaller PCC (Fig. 4). This can be readily explained by the presence of bleached GFPn also

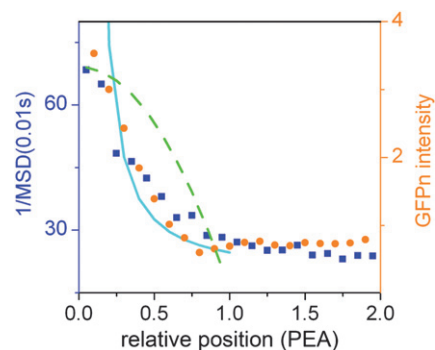


Fig. 4 The averaged fluorescent intensity is correlated to the HA concentration which should be inversely related to the averaged MSD. The green (thick, dashed) line depicts the relative parabolic concentration profile predicted by Milner *et al.* for an end-grafted polymer brush.³⁵ The light blue line depicts the $z^{-4/3}$ curve for the self-similar carpet model predicted by de Gennes³⁷ for adsorbed polymers.

binding to HA and the resolution limit making it impossible to distinguish the small amounts of GFPn on the PCC fringe against the noise level. The GFPn staining therefore does not yield information about the outer edge of the PCC. Micro-rheology measurements, on the other hand, are very sensitive to slight variations in viscoelasticity. They seem to indicate a somewhat larger PCC than the PEA. The PEA defines the edge of the PCC by the ability of erythrocytes to approach the cell. They are stopped at a distance where the PCC forms an impenetrable barrier to them. Due to the gradient nature of this barrier the erythrocytes might be able to penetrate the outer fringes of the PCC, where the edge so-defined will be reproducible, but somewhat smaller than that measurable by the more sensitive passive microrheology technique.

Hyaluronan profiles in the PCC

Labeling cells with GFPn successfully stained the hyaluronan within the PCC. This treatment did not harm the living cells and did not seem to alter the PCC since no change in thickness was observed as measured by PEA. However, any interactions of the cell with HA might be influenced by the GFPn attachment, possibly leading to a modified uptake of hyaluronan or a modified cell response. To exclude or at least minimize such long-term effects, we performed all fluorescence experiments immediately after GFPn addition.

GFPn staining outside of cells is subject to a high photobleaching rate, readily observed in standard fluorescent and confocal laser scanning microscope. This effect is considerably reduced in spinning disk microscopy which yields reproducible intensity profiles within one sample at the same settings. In addition to photobleaching, we expect that parts of HA might be blocked by other hyaluronan-binding proteins. The GFPn intensity can therefore not be correlated to an absolute HA concentration. Thus relative maps of the hyaluronan distribution within the PCC are obtainable with spinning disk microscopy.

The qualitative agreement of the HA's concentration profile with its mechanical profile relies upon the assumption that the GFPn intensity is directly proportional to the local HA concentration. This implicitly assumes that the probability of GFPn binding to an HA molecule does not depend on its location in the coat matrix, which suggests that any coat proteins are uniformly distributed along the HA chains. We note that this same assumption also led to the useful observation that rescaling our data with respect to the relative position in the cell coat, p , allowed us to compare data from different cells with different PCC thicknesses in one comprehensive plot. The rescaling of the data led to the clear linear increase in the MSD and the diffusive exponent, α , with respect to relative position away from the cell (Fig. 2). Our self-consistent results imply that our assumption that the hyaluronan-binding proteins are uniformly distributed along the HA chains is reasonable. However, thorough investigation of this delicate issue is beyond the scope of this work and should be addressed in a future, more biologically oriented work. Here we emphasize that the general correlation of the two distinct experimental profiles is an interesting observation and presents a unique approach to relate structure and mechanics of extended polymer films using quantitative fluorescence combined with particle tracking microrheology techniques.

Macromolecular organization of the PCC

A key question regarding hyaluronan-rich pericellular coats concerns the origin of their extended matrices. Although hyaluronan can have extremely long contour lengths of several micrometres, even the largest molecule has a radius of gyration in the sub-micron range. Therefore "some kind of brush formation of the hyaluronan chains"¹ is predicted for a PCC thickness of several micrometres. This implies a scenario where grafted HA polymers are stretched out to considerably more than their native radius of gyration.

In general, density profiles of grafted polymers can be related to their organization and structure at the surface. Our profile of the HA concentration within the PCC and its validation by its agreement with our mechanical measurements provide a first opportunity to consider directly whether the polymer brush hypothesis can be applied to RCJ-P cells. The density profile, φ , of end-grafted polymer brushes in the Alexander–de Gennes model is constant and scales with their height, as $\varphi \approx H^2$,^{33,34} where H is the thickness of the layer corresponding to the parameter t in our systems. Milner *et al.*³⁵ introduced corrections to this model that have been verified experimentally, showing that the density profile scales parabolically with distance to the cell surface such that $\varphi(z) \approx H^2 - z^2$, where z is the distance to the grafting surface, corresponding to the relative position, p . Comparing this parabolic profile (Fig. 4) with the measured concentration profile, we find no agreement with our measured concentration profiles.

In contrast to these theories, the biological organization of hyaluronan molecules within the PCC is far more complex. HA is most likely not monodisperse since hyaluronan synthases produce hyaluronan with a certain length range.³⁶ They are not just attached by their ends, since surface receptors such as CD44 can bind HA anywhere along the chain. Thus the organization of HA is more similar to de Gennes' self-similar carpet model of adsorbed polymers to surface.³⁷ The amount of HA receptors would thus influence the preference of HA towards the surface. The predicted concentration profile for adsorbed polymers in this model, which scales as $\varphi \approx z^{-4/3}$, corresponds qualitatively well with our observed profile scaling (Fig. 4). Additionally the attachment of hyaluronan-binding proteins changes the local polymer properties and hyaluronan-binding proteins might change HA's size and shape, as their attachment could lead to a further stretching of the chains.³⁸ It is thus remarkable that such a dynamic system shows reproducible profiles within our observation time window.

Materials and methods

Reagents

All reagents were purchased from Gibco unless stated otherwise. Hyaluronidase (from *Streptomyces hyalurolyticus*) was purchased from Seigagaku and Alexa Fluor 555 labelled wheat germ agglutinin (WGA555) and carbocyanine dye DiI from Invitrogen.

Cell culture

Rat chondrocyte cells RCJ-P (from foetal calvaria, batch 15.01.98; Prochon Biotech, Rehovot, Israel) were cultured in

MEM α medium supplemented with 15% FBS and 2% L-glutamine at 37 °C in 5% CO₂. 6 h before each experiment, cells were trypsinised and plated on glass cover slides fixed to home-built Teflon holders with vacuum grease.

Hyaluronidase treatment

Adhered cells were incubated for 15 min in a 1 : 20 mixture of hyaluronidase solution in culture medium, rinsed twice and supplemented with fresh media.

Particle exclusion assay (PEA)

Fresh pig blood (slaughterhouse “Fleischversorgungs-zentrum”, Mannheim) was immediately supplemented with EDTA to a final concentration of 1.5 mg ml⁻¹ and kept at 4 °C. Erythrocytes were extracted and used following standard procedures.³⁹

GFPn purification

Transfected HEK cells were cultivated according to Zhang and co-workers.²⁹ The growth medium was partly replaced every two days. The supernatant was centrifuged, supplemented with protease inhibitor cocktail (Roche) and incubated with Ni-NTA agarose beads (Qiagen) in a rotary wheel at 4 °C overnight and transferred to a polypropylene column (Qiagen). Unspecifically bound protein was removed with washing buffer containing 20 mM imidazole. The fusion protein was subsequently eluted with buffer containing 250 mM imidazole.

Blocking GFPn with short HA

The specific binding of GFPn to HA can be controlled by specifically blocking GFPn with short HA (of a unit length of 8 disaccharides). GFPn was incubated in an excess of short HA (Hyalose) for 30 min.

Spinning disk microscopy

The confocal spinning disk experiments were performed on an AxioVert200 M (Zeiss) equipped with a Perkin-Elmer Ultraview ER System with an Ar/Kr-laser at 488 nm and 568 nm wavelengths and a water immersion objective (Zeiss, C-Apochromat, 40 \times , NA = 1.1). The cell membrane and the erythrocytes were labelled using WGA555 and DiI, and the hyaluronan was labelled using the GFPn fusion protein. Images were taken 4 μ m above the surface with an ORCA-ER CCD camera (Hamamatsu) at an exposure times of 200 ms (568 nm) and 2500 ms (488 nm). Fluorescent profiles of the PCC were chosen perpendicular to the cell surface summed over a width of 10 pixels to reduce noise, where the fluorescent image of the membrane was used to determine the location of the cell surface, which was set to zero in the PCC profile.

Microrheology (MR)

The Brownian motion of carboxylated, YG polystyrene latex spheres with a diameter of 0.45 μ m (Polysciences, Inc.) was observed on an AxioVert200 M microscope through a glycerine immersion objective (Zeiss, Plan-Neofluar, 63 \times , NA = 1.3) equipped with a heatable stage set to 37 °C. The particles were

visualized in fluorescent mode with an eGFP filter (Zeiss, no. 38). The cell sample was equilibrated for 10 min on the microscope stage before 10 μ L of the ultrasound treated (1 min) tracer solution were added which were allowed to diffuse into the PCC and equilibrate for 15 min.

In a typical experiment, the motion of the tracer particles was recorded with the Phantom 7.2 camera (Vision Research) at a frame rate of 500 fps over 8000 frames. Afterwards, erythrocytes were added and the PEA was observed with an ORCA-ER CCD camera. The acquired images were analyzed with the software package IDL (Research Systems Inc.) based on the algorithms developed by Crocker and Grier.⁴⁰ Tracer particles that were either agglomerated, visible for less than 650 frames, phagocytosed, close to a part of the cell surface with high curvature or above a filopodia were excluded from analysis.

The Brownian motion of individual tracers is characterized by their mean-square displacement (MSD), defined as:

$$\text{MSD} = \langle \Delta \bar{r}(\tau) \rangle = \left\langle |\bar{r}(t + \tau) - \bar{r}(t)|^2 \right\rangle \quad (2)$$

where \bar{r} is the n -dimensional (here $n = 2$) particle position, τ is the lag time and the brackets indicate an average over all times t .

The MSD value at a certain lag time and its diffusion exponent, α , corresponding to the double-logarithmic slope of the MSD, can be measured and used to calculate the storage modulus (G') and the loss modulus (G'') of the embedding solution:^{30,41,42}

$$\begin{aligned} G'(\omega) &= G(\omega) \cos[\pi\alpha(\omega)/2] \\ G''(\omega) &= G(\omega) \sin[\pi\alpha(\omega)/2] \end{aligned} \quad (3)$$

$$\text{where } G(\omega) = \frac{k_B T}{\pi r \langle \text{MSD}(1/\omega) \rangle \Gamma[1 + \alpha(\omega)]} \quad (4)$$

where $\omega = 1/\tau$ and Γ is the gamma function. We calculated the two-dimensional MSD of each single track and subsequently multiplied its value by 3/2 to obtain the three-dimensional MSD.⁴² In order to obtain the diffusive exponent, α , corresponding to the double-logarithmic slope at $\tau = 0.01$ s, we fitted the data between 0.006 s and 0.014 s. The chosen τ value is short enough to ensure good statistics as $\tau \ll t_{\text{max}}$. The position of each particle was estimated to be as the “centre of mass” of its trajectory during the recording time. The relative position of each particle with respect to the cell membrane (by definition, set to zero) and the edge of the PCC (set to one) were determined on the PEA image. The weighted diffusive exponent α_w takes the number of frames, n , for each track, i , at a given window of relative position, p ($\Delta = 0, 1$), into account:

$$\alpha_w(\omega, p) = \frac{\sum_i n_i \alpha(\omega, p)_i}{\sum_i n_i} \quad (5)$$

Conclusions

In conclusion, we present two independent techniques for characterizing the pericellular coat on living cells. HA distribution profiles were obtained with GFPn in spinning disk microscopy. The micromechanical structure was measured unobtrusively with

passive particle tracking microrheology. The two profiles can be correlated by defining the relative position of the PCC *via* PEA. It can be shown that the two profiles agree well with one another in accordance with the modified Rouse model. The observed HA concentration gradient and mechanical properties might play an unconsidered role in the mechanical interactions with the extracellular matrix or other cells. Since both techniques are independent of changes in the adjacent cell mechanics, we introduce the tools that have been lacking for comparison of PCCs, as required for understanding the effects on the PCC by drugs or hyaluronan-binding proteins as well as the alterations in osteoarthritic or aged cells.

Acknowledgements

We greatly appreciate the gift of RCJ-P cells from Prof. B. Geiger (Weizman Inst., Rehovot, Israel). We would like to give our thanks to Victor Breedveld and Ralf Richter for inspiring discussions, to Martin Etzrodt, Peter Kaiser and the Nikon Center for technical assistance and to Richard Seager for his help in writing. We thank the Max Planck Society for generous financial support. JEC was also funded by an Alexander von Humboldt Fellowship and Georgia Institute of Technology start up funds.

References

- 1 S. P. Evanko, M. I. Tammi, R. H. Tammi and T. N. Wight, *Adv. Drug Delivery Rev.*, 2007, **59**, 1351–1365.
- 2 M. Cohen, Z. Kam, L. Addadi and B. Geiger, *EMBO J.*, 2006, **25**, 302–311.
- 3 S. P. Evanko, J. C. Angello and T. N. Wight, *Arterioscler., Thromb., Vasc. Biol.*, 1999, **19**, 1004–1013.
- 4 H. Chao and A. P. Spicer, *J. Biol. Chem.*, 2005, **280**, 27513–27522.
- 5 N. Itano, F. Atsumi, T. Sawai, Y. Yamada, O. Miyaishi, T. Senga, M. Hamaguchi and K. Kimata, *Proc. Natl. Acad. Sci. U. S. A.*, 2002, **99**, 3609–3614.
- 6 C. Ricciardelli, D. L. Russell, M. P. Ween, K. Mayne, S. Suwiat, S. Byers, V. R. Marshall, W. D. Tilley and D. J. Horsfall, *J. Biol. Chem.*, 2007, **282**, 10814–10825.
- 7 B. Toole, *Semin. Cell Dev. Biol.*, 2001, **12**, 79–87.
- 8 K. Rilla, R. Tiihonen, A. Kultti, M. Tammi and R. H. Tammi, *J. Histochem. Cytochem.*, 2008, **56**, 901–910.
- 9 A. J. Day and G. D. Prestwich, *J. Biol. Chem.*, 2002, **277**, 4585–4588.
- 10 B. P. Toole, *Nat. Rev. Cancer*, 2004, **4**, 528–539.
- 11 G. M. Lee, B. Johnstone, K. Jacobson and B. Caterson, *J. Cell Biol.*, 1993, **123**, 1899–1907.
- 12 L. Alexopoulos, L. Setton and F. Guilak, *Acta Biomater.*, 2005, **1**, 317–325.
- 13 J. Dudhia, C. M. Davidson, T. M. Wells, D. H. Vynios, T. E. Hardingham and M. T. Bayliss, *Biochem. J.*, 1996, **313**, 933–940.
- 14 G. Verbruggen, M. Cornelissen, K. F. Almqvist, L. Wang, D. Elewaut, C. Broddelez, L. de Ridder and E. M. Veys, *Osteoarthr. Cartilage*, 2000, **8**, 170–179.
- 15 G. Rizkalla, A. Reiner, E. Bogoch and A. R. Poole, *J. Clin. Invest.*, 1992, **90**, 2268–2277.
- 16 P. M. Freeman, R. N. Natarajan, J. H. Kimura and T. P. Andriacchi, *J. Orthop. Res.*, 1994, **12**, 311–320.
- 17 M. Knight, S. Ghori, D. Lee and D. Bader, *Med. Eng. Phys.*, 1998, **20**, 684–688.
- 18 W. Trickey, F. Baaijens, T. Laursen, L. Alexopoulos and F. Guilak, *J. Biomechanics*, 2006, **39**, 78–87.
- 19 L. Alexopoulos, G. Williams, M. Ugpton, L. Setton and F. Guilak, *J. Biomechanics*, 2005, **38**, 509–517.
- 20 D. L. Bader, T. Ohashi, M. M. Knight, D. A. Lee and M. Sato, *Biorheology*, 2002, **39**, 69–78.
- 21 L. Ng, H. Hung, A. Sprunt, S. Chubinskaya, C. Ortiz and A. Grodzinsky, *J. Biomechanics*, 2007, **40**, 1011–1023.
- 22 I. Sokolov, S. Iyer, V. Subba-Rao, R. M. Gaikwad and C. D. Woodworth, *Appl. Phys. Lett.*, 2007, **91**, 023902.
- 23 M. Cohen, E. Klein, B. Geiger and L. Addadi, *Biophys. J.*, 2003, **85**, 1996–2005.
- 24 M. Gardel, M. Valentine and D. Weitz, *Microscale Diagnostic Techniques*, Springer, Heidelberg, 2005, Microrheology chapter.
- 25 T. A. Waigh, *Rep. Prog. Phys.*, 2005, **68**, 685–742.
- 26 W. Krause, E. Bellomo and R. Colby, *Biomacromolecules*, 2001, **2**, 65–69.
- 27 I. Y. Wong, M. L. Gardel, D. R. Reichman, E. R. Weeks, M. T. Valentine, A. R. Bausch and D. A. Weitz, *Phys. Rev. Lett.*, 2004, **92**, 178101.
- 28 J. Sato and V. Breedveld, *J. Rheol. (N. Y.)*, 2005, **50**, 1–19.
- 29 H. Zhang, S. L. Baader, M. Sixt, J. Kappler and U. Rauch, *J. Histochem. Cytochem.*, 2004, **52**, 915–922.
- 30 T. Mason, *Rheol. Acta*, 2000, **39**, 371–378.
- 31 D. Calciu-Rusu, E. Rothfuss, J. Eckelt, T. Haase, H. B. Dick and B. A. Wolf, *Biomacromolecules*, 2007, **8**, 1287–1292.
- 32 A. Papagiannopoulos, T. A. Waigh and T. E. Hardingham, *Faraday Discuss.*, 2008, **139**, 1–22.
- 33 P.-G. de Gennes, *J. Phys. (Les Ulis, Fr.)*, 1976, **37**, 1445–1452.
- 34 S. Alexander, *J. Phys. (Les Ulis, Fr.)*, 1977, **38**, 983.
- 35 S. T. Milner, T. A. Witten and M. E. Cates, *Macromolecules*, 1998, **21**, 2610–2619.
- 36 P. DeAngelis, *Cell. Mol. Life Sci.*, 1999, **56**, 670–682.
- 37 P.-G. de Gennes, *Adv. Colloid Interface Sci.*, 1987, **27**, 189–209.
- 38 M. Hellmann, M. Weiss and D. W. Heermann, *Phys. Rev. E: Stat. Phys., Plasmas, Fluids, Relat. Interdiscip. Top.*, 2007, **76**, 021802.
- 39 B. J. Clarris and J. R. Fraser, *Exp. Cell Res.*, 1968, **49**, 181–93.
- 40 J. Crocker and D. G. Grier, *J. Colloid Interface Sci.*, 1996, **179**, 298–310.
- 41 T. Mason and D. Weitz, *Phys. Rev. Lett.*, 1995, **74**, 1250–1253.
- 42 T. Mason, K. Ganesan, J. van Zanten, D. Wirtz and S. Kuo, *Phys. Rev. Lett.*, 1997, **79**, 3282–3285.